Carbon-Hydrogen Bond Breaking and Making in the Open-Shell Singlet Molecule Cp* 2 Yb(4,7-Me 2 phen)

Grégory A Nocton, Corwin A Booth, Laurent Maron, Louis Ricard, Richard A Andersen

Carbon-Hydrogen Bond Breaking and Making in the Open-Shell Singlet Molecule, $Cp^*_2Yb(4,7\text{-}Me_2phen)$

Grégory Nocton,*[†‡] Corwin H. Booth,[§] Laurent Maron,[⊥] Louis Ricard,[†] and Richard A. Andersen.*[‡§]

[†] *Laboratoire de Chimie Moléculaire, CNRS, Ecole Polytechnique, Palaiseau, France.*
[‡] *Department of Chemistry, University of California, Berkeley, California 94720*
[§] *Chemical Sciences Division, Lawrence Berkeley National Laboratory, Berkeley, CA 94720*
[⊥] *LPCNO, UMR 5215, Université de Toulouse-CNRS, INSA, UPS, Toulouse, France*

Supporting Information Placeholder

ABSTRACT: The adducts formed between the 4,7-Me_2, 3,4,7,8-Me_4, 3,4,5,6,7,8-Me_6-phenanthroline ligands and Cp^*_2Yb are shown to have open-shell singlet ground states by magnetic susceptibility and L_{III}-edge XANES spectroscopy. Variable temperature XANES data show that two singlet states are occupied in each adduct that are fit to a Boltzmann distribution for which $\Delta H = 5.75$ kJ.mol^{-1} for the 4,7-Me_2phen adduct. The results of a CASSCF calculation for the 4,7-Me_2phen adduct indicates that three open-shell singlet states, SS1, SS2, and SS3 lie 0.44 eV, 0.06 EV and 0.02 eV, respectively, below the triplet state. These results are in dramatic contrast to those acquired for the phenanthroline and 5,6-Me_2phen adducts that are ground state triplets (*J. Am Chem. Soc.*, **2014**, *136*, 8626). A model that accounts for these differences is traced to the relative energies of the LUMO and LUMO+1 orbitals that depend on the position the methyl group occupies in the phenanthroline ligand. The model also accounts for the difference in reactivity of Cp^*_2Yb(3,8-Me_2phen) and Cp^*_2Yb(4,7-Me_2phen); the former forms a σ C-C bond between C(4)C(4') and the latter undergoes C-H bond cleavage at the methyl group on C(4) and leads to two products that co-crystallize: Cp^*_2Yb(4-(CH_2),7-Mephen), which has lost an hydrogen atom and Cp^*_2Yb(4,7-Me_2-*4H*-phen), which has gained an hydrogen atom.

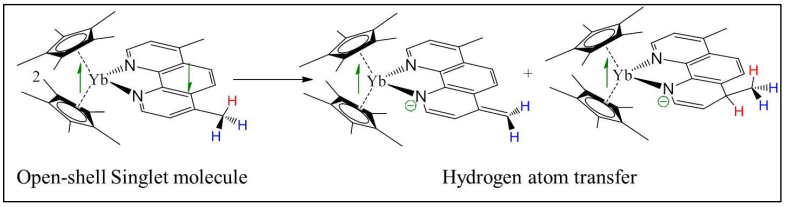

INTRODUCTION.

The ground state electronic structure of the neutral 2,2'-bipyridine and some 1,10-phenanthroline adducts of Cp^*_2Yb, Cp^*_2Yb(diimine), has been studied with the goal of understanding the fundamental nature of how the spin on the f^{13} fragment couples with the electron in the diimine LUMO of these paramagnetic compounds. The bipyridine adducts are open-shell singlet molecules that result when an open-shell singlet configuration couples with the closed-shell singlet configuration, driving the energy of the resultant singlet state below the triplet state, in violation of Hund's maximum multiplicity rules. These states are multiconfigurational, the spins are antiferromagnetically coupled, and the valence of ytterbium is intermediate, *i.e.* it lies between Yb(II), f^{14}, and Yb(III), f^{13}.[1-5] In contrast, when the diimine is a phenanthroline ligand, x,x'-Me_2phen, where x,x' is H,H, 3,8-Me_2 or 5,6-Me_2, the ground state is a spin triplet in which the spins on the individual fragments are ferromagnetically coupled and the valence is fully trivalent, Yb(III), f^{13}.[6] In these phenanthroline adducts, when x,x' is H,H or 3,8-Me_2, the monomeric units couple by forming a σ C-C bond between the C(4)C(4') atoms and the Cp^*_2Yb(III), f^{13}, fragments are isolated paramagnetic $Cp^*_2Yb^+$ groups bridged by the resulting diamagnetic dianion. The C–C bonds in these dimers are weak and in solution a dimer – monomer equilibrium exists in which $\Delta G \approx 0$ when x,x' is 3,8-Me_2.

In this article, it is shown that the ground state electronic structure of the 4,7-Me_2phen adduct of Cp^*_2Yb is an open-shell singlet like those for bipyridine, which is in contrast to the triplet ground state when x,x'-phen is H,H, 3,8Me_2 or 5,6-Me_2. The different behavior of substituted phenantholines has it origin in the ground state of their solvent-separated radical anions, as determined by analysis of their EPR spectra. Thus, the radical anions of bipy$^{\cdot-}$, 4,4'-Me_2bipy$^{\cdot-}$, and 5,5'-Me_2bipy$^{\cdot-}$,[7] phen$^{\cdot-}$,[7] 2,9-Me_2phen$^{\cdot-}$,[8] 4,7-Me_2phen$^{\cdot-}$[7] and 5,6-Me_2phen$^{\cdot-}$[8] have $^2B_1$ ground states but 3,4,7,8-Me_4phen$^{\cdot-}$ has a $^2A_2$ ground state.[9] The influence of the electronic structure of the diimine radical anion on the physical and chemical properties is illustrated by the following example: Cp_2Ti(bipy) is a spin equilibrium adduct in which the ground state singlet is in equilibrium with a triplet excited state with $-2J \approx 600$ cm^{-1}.[10] Although the spin state of Cp_2Ti(phen) is unknown, the 3,4,7,8-Me_4phen derivative disproportionates according to the reaction illustrated in Scheme 1.[11] These titanocene results set the stage for the decamethylytterbocene chemistry that follows.

Scheme 1.[11]

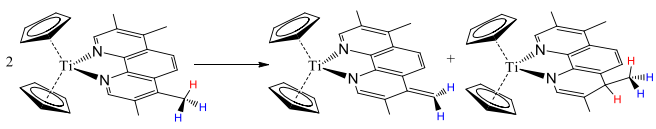

Table 1. Solid state properties of the compounds **1-6**. The atom numbering scheme for the phenanthroline is in scheme 2.

Compound	color	m.p (°C)	IR (cm^{-1})	μ_{eff} (300K)[a]
$Cp^*_2Yb(2,9\text{-}Me_2phen)$ (**1**)	deep purple	313-317	1622, 1592, 1505, 848	1.62
$Cp^*_2Yb(4,7\text{-}Me_2phen)$ (**2**)	deep purple	265-268	1622, 1577, 1520, 849	1.98
$Cp^*_2Yb(3,4,7,8\text{-}Me_4phen)$ (**3**)	dark brown	264-266	1611, 1567, 1518, 810	1.79
$Cp^*_2Yb(3,4,5,6,7,8\text{-}Me_6phen)$ (**4**)	dark brown	270-272	-	1.67
$Cp^*_2Yb(2,9\text{-}Me_2\text{-}4,7\text{-}Ph_2phen)$ (**5**)	dark purple	288-292	1622, 1569,1547, 880	2.05
$[Cp^*_2Yb(4,7\text{-}Me_2phen)]I$ (**6**)	gold yellow	214-218	1631, 1534, 1430, 728	4.44
$Cp^*_2Yb(5,6\text{-}Me_2phen)$[6]	deep purple	285-287	1605, 1584, 1480, 804	3.68

a) In μ_B per Yb(III), calculated from a plot of χT vs T, where $\mu_{eff} = 2.828\ (\chi T)^{1/2}$ at T = 300 K.

RESULTS.

Synthesis and Physical Properties. The substituted phenanthroline adducts are prepared as illustrated in eq. 1. Some physical properties of the adducts prepared in this article are given in Table 1.

$$Cp^*_2Yb(OEt_2) + x,x'\text{-phen} \longrightarrow Cp^*_2Yb(x,x'\text{-phen}) + Et_2O \qquad \textbf{Eq. 1}$$

All the adducts are soluble in either toluene or diethylether from which they are purified, in most cases, by crystallization at low temperature. The good solubility of the neutral adducts is in contrast to the solubility of $Cp^*_2Yb(x\text{-phen})$, where x is H,[5] 3-Me, 4-Me, 5-Me, which are only sparingly soluble in these solvents.[6] All of the adducts are high melting point solids that are thermally stable in solution, except for the 4,7-Me_2, 3,4,7,8-Me_4, and 3,4,5,6,7,8-Me_6 phenanthroline adducts that are best prepared and isolated at 0 °C or below; the thermal rearrangement of these adducts is described below.

Scheme 2.

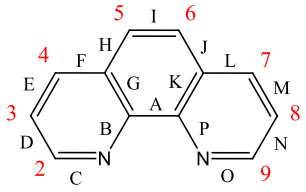

The effective magnetic moments of these adducts in the solid state at 300 K are substantially lower than in the x-phen adducts mentioned above and in $Cp^*_2Yb(5,6\text{-}Me_2phen)$,[6] and lower than expected for two uncorrelated spins of Yb(III), f^{13} and a radical anion of $^2F_{7/2}$ and $^2S_{1/2}$, respectively, for which a μ_{eff} value of 4.85 μ_B is expected. However, the value for the cation, $[Cp^*_2Yb(4,7\text{-}Me_2phen)]I$, **6**, is as expected for an isolated $^2F_{7/2}$, Yb(III) paramagnetic compound of 4.54 μ_B. The lower effective magnetic moments at 300 K for the adducts given in Table 1 clearly show that the spins are correlated and that antiferromagnetic coupling is greater when two methyl groups occupy the 4 and 7-positions in the phenanthroline ring, in contrast to when they occupy the 3,8- or 5,6- positions.

The temperature dependence of the effective magnetic moments in the solid state is shown in Figure 1, the plots of χ, χ^{-1} and χT vs. T are available in SI. These plots clearly illustrate the reduced moments of the neutral adducts compared to $Cp^*_2Yb(5,6\text{-}Me_2phen)$ and $[Cp^*_2Yb(4,7\text{-}Me_2phen)]I$, **6**. In all cases, the general shape of the curves is similar for the neutral adducts, μ_{eff} decreasing rapidly below ca. 25 K, indicating either a change in population of the crystal field states, since the crystal field splitting is small, and/or an intermediate valent nature of the ground state, as observed in the neutral methyl substituted bipyridine adducts of Cp^*_2Yb for which the relative f^{13} to f^{14} configuration fractions depend on temperature.[3]

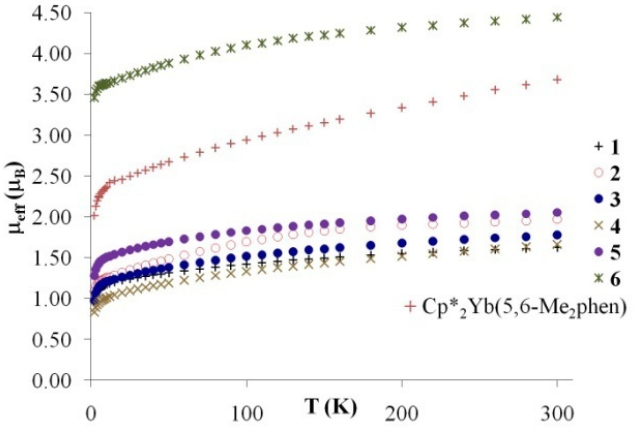

Figure 1. Temperature dependent magnetic data for **1-6** and $Cp^*_2Yb(5,6\text{-}Me_2phen)$.[6]

Table 2. Thermodynamic constants derived for the SS1 ⇌ SS2 equilibrium from n_f *vs.* T and χ *vs.* T plots (Figure 3).

Compound	$n_{f(gs)}$	$n_{f(ex)}$	$\chi_{(gs)}$[a]	$\chi_{(ex)}$[a]	$\Delta H_{(nf)}$[b]	$\Delta H_{(\chi)}$[b]	$\Delta S_{(nf)}$[c]	$\Delta S_{(\chi)}$[c]	%imp
$Cp^*_2Yb(4,7\text{-}Me_2phen)$ (**2**)	0.81	0.58	0.00182	0.00060	5.75	5.75	31	25	7.0
$Cp^*_2Yb(3,4,7,8\text{-}Me_4phen)$ (**3**)	0.61	0.50	0.00125	0.00060	3.2	3.6	21	21	6.8
$Cp^*_2Yb(3,4,5,6,7,8\text{-}Me_6phen)$ (**4**)	0.37	0.27	0.000108	0.00062	3.0	3.9	25	21	4.7

a) $emu.mol^{-1}$ b) $kJ.mol^{-1}$ c) $J.(mol.K)^{-1}$

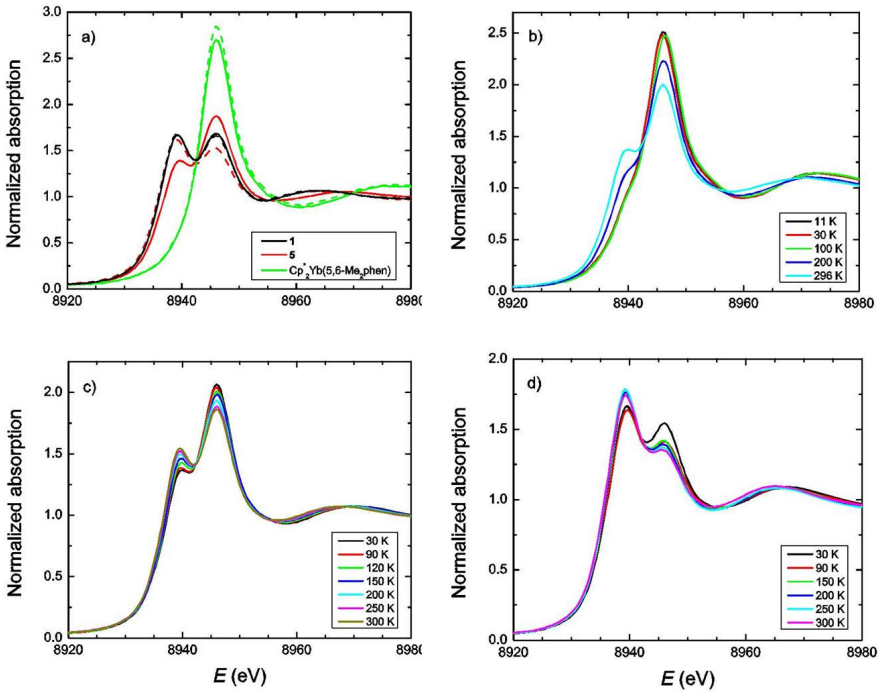

Figure 2: Yb L_{III}-edge XANES data for the complexes a) $Cp^*_2Yb(2,9\text{-}Me_2phen)$, **1**, $Cp^*_2Yb(2,9\text{-}Me_2,4,7\text{-}Ph_2phen)$, **5**, and $Cp^*_2Yb(5,6\text{-}Me_2phen)$[6] at 300 K (dashed) and 30 K (solid). b) $Cp^*_2Yb(4,7\text{-}Me_2phen)$, **2,** at various temperatures, c) $Cp^*_2Yb(3,4,7,8\text{-}Me_4phen)$, **3,** at various temperatures and d) $Cp^*_2Yb(3,4,5,6,7,8\text{-}Me_6phen)$, **4,** at various temperatures.

The L_{III}-edge XANES spectra are able to distinguish between these two possibilities. In contrast to $Cp^*_2Yb(5,6\text{-}Me_2phen)$, which shows only one temperature-independent f^{13} feature at 8946 eV (Figure 2a), $Cp^*_2Yb(4,7\text{-}Me_2phen)$, **2**, presents two different features, in agreement with the presence of both f^{14} and f^{13} contributions, for which the intensity ratio changes with the temperature (Figure 2b). This situation was observed in previous work with some substituted bipy adducts[3] when the ligand can accept the electron from Yb in Cp^*_2Yb into several accessible π^* orbitals (π^*_1, π^*_2, ...), which results in several possible open-shell singlets in which both the relative π^* contribution and the f^{13}:f^{14} ratio are different, accounting for the temperature dependence in the L_{III}-XANES spectra. For $[Cp^*_2Yb(4,7\text{-}Me_2phen)]$, **2,** the f^{13} configuration fraction (also known as the relative f^{13} occupancy or the f-hole occupancy, n_f) varies from 0.81 at low temperature to 0.58 at 296 K. This situation also accounts for the low magnetic moment of $Cp^*_2Yb(4,7\text{-}Me_2phen)]$, **2**. When the number of methyl groups is increased in the phenanthroline ligand, the f^{13}:f^{14} ratio decreases and the spectra continue to show a temperature dependence.

In the Cp^*_2Yb adducts with substituted bipyridine ligands, the temperature dependence is due to the presence of several open-shell singlet states (SS) that develop below the triplet (T) and it is therefore possible to determine their relative population using a Boltzmann equation.[3] A similar methodology is used in this work for $Cp^*_2Yb(4,7\text{-}Me_2phen)$, **2**; $Cp^*_2Yb(3,4,7,8\text{-}Me_4phen)$, **3**; $Cp^*_2Yb(3,4,5,6,7,8\text{-}Me_6phen)$, **4** and the fits are presented in Figure 3, while the parameters are reported in Table 2. Only two singlet states, SS1 and SS2, are used in all three complexes. In the same manner, the magnetic curves are fit (Figure 3) with a Boltzmann distribution of two open-shell singlet states below the triplet and the enthalpy and entropy changes obtained from both fits (XANES and magnetism) agree well. The enthalpy change for $Cp^*_2Yb(4,7\text{-}Me_2phen)$, **2**, is 5.75 $kJ.mol^{-1}$ and lies in the reported range for the enthalpy changes in substituted bipyridine adducts of Cp^*_2Yb. As an additional note, the percentage of $^2F_{7/2}$ impurties used for the fit of the magnetic data is relatively high, compared to previous work, but is rationalized by the thermal instability of **2-4** (see Reactivity Section). The L_{III}-edge XANES data give n_f values of 0.41 and 0.55 at 30 K for $Cp^*_2Yb(2,9\text{-}Me_2phen)$ **1**, and $Cp^*_2Yb(2,9\text{-}Me_2\text{-}4,7\text{-}Ph_2phen)$ **5**, respectively, and show no temperature dependence for $Cp^*_2Yb(2,9\text{-}Me_2phen)$, **1**, while n_f decreases to 0.37 at 300 K for $Cp^*_2Yb(2,9\text{-}Me_2\text{-}4,7\text{-}Ph_2phen)$, **5**. The reason for the low n_f values and variable temperature behavior of these two complexes is not addressed in a quantitative manner in this work but the general behavior is similar to that of $Cp^*_2Yb(6,6'\text{-}Me_2bipy)$ and $Cp^*_2Yb(6\text{-}Mebipy)$, respectively;[3] the presence of a methyl group(s) in the α position to nitrogen destabilizes the f^{13} configuration, presumably because of the steric hindrance. The low values of n_f for **1** and **5** also account for the low values of effective moments (see Table 1, $n_f = 0$ indicates diamagnetic f^{14}) and for the chemical shift in their solution ^1H NMR spectra.

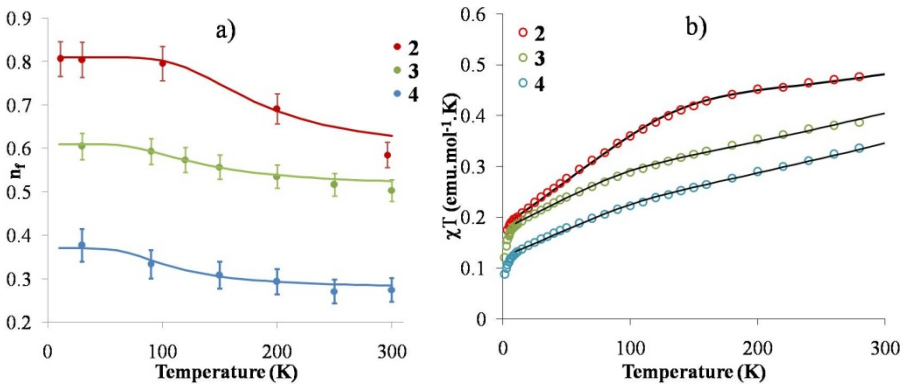

Figure 3: a) Plot of n_f vs. T (K) for **2-4**. The best fits are obtained from a Boltzmann distribution between two singlet states using the parameters reported in Table 2. b) Plot of χT *vs.* temperature for complexes **2-4**. The black lines for each compound show the fit to the data using the parameters reported in Table 3.

X-ray crystallography. The ORTEPs of $Cp^*_2Yb(4,7\text{-}Me_2phen)$, **2**, and $Cp^*_2Yb(2,9\text{-}Me_2\text{-}4,7\text{-}Ph_2phen)$, **5**, are shown in Figure 4 and Figure 5, respectively. Some bond lengths and angles are given in Table 3 and crystal data are in the Experimental Section and SI. It is clear that these two adducts are monomers in the solid state, in contrast to the phenanthroline and 3,8-Me_2phen adducts.[6] The average Yb-C(Cp*) distance in $Cp^*_2Yb(4,7\text{-}Me_2phen)$ of 2.642 ± 0.007 Å is 0.032 Å and 0.020 Å longer than the equivalent distances in $Cp^*_2Yb(phen)$ monomer and in the four molecules in the two crystal structures of $Cp^*_2Yb(5,6\text{-}Me_2phen)$, respectively. The Yb-N distances follow a similar pattern; the distance in $Cp^*_2Yb(4,7\text{-}Me_2phen)$ is 0.035 Å and 0.030 Å longer than the equivalent distances in $Cp^*_2Yb(phen)$ monomer and $Cp^*_2Yb(5,6\text{-}Me_2phen)$, respectively. The Yb-C(Cp*) and Yb-N distances in $Cp^*_2Yb(2,9\text{-}Me_2\text{-}4,7\text{-}Ph_2phen)$, **5**, are 0.098 Å and 0.16 Å, respectively, much longer than equivalent distances in $Cp^*_2Yb(4,7\text{-}Me_2phen)$, **2**, and close to the equivalent distances in $Cp^*_2Yb(py)_2$ of 2.74 Å and 2.565 ± 0.005 Å, respectively.[12] The longer Yb-C(Cp*) and Yb-N distances at 173 K in **2** and **5**, relative to these distances in $Cp^*_2Yb(phen)$ and $Cp^*_2Yb(5,6\text{-}Me_2phen)$[6], indicate that the population of the Yb(II, f^{14}) configuration is greater in the former adducts, consistent with the lower values of n_f.

Table 3. Selected bond distances (Å) and angles (°) at 173 K for complexes **2** and **5**.

	$Cp^*_2Yb(4,7\text{-}Me_2phen)$ (**2**)	$Cp^*_2Yb(2,9\text{-}Me_2\text{-}4,7\text{-}Ph_2phen)$ (**5**)
Yb-C (distances range)	2.630(4) – 2.653(4)	2.699(10) – 2.781(7)
Yb-C(ring) (mean)	2.642 ± 0.007	2.74 ± 0.02
Yb-C_t (mean)[a]	2.35	2.46
C_t-Yb-C_t [a]	139.5	140.0
Yb-N(mean)	2.35 ± 0.01	2.51 ± 0.002
C(23)-C_{exo}[b]	1.486(6)	1.496(9)
C(28)-C_{exo} [c]	1.507(5)	1.506(9)
torsion angle N-C-C-N	1	3
torsion angle C-C-C-C	1	1

a) C_t is the centroid of the C_5Me_5 ring b) C_{exo} in **2** is C(33) and C(35) in **5** c) C_{exo} is C(34) in **2** and C(41) in **5**

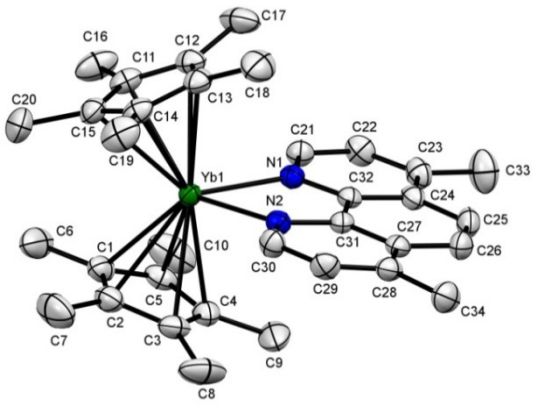

Figure 4. ORTEP for the complex $Cp^*_2Yb(4,7\text{-}Me_2phen)$ (**2**). (Thermal ellipsoids are at 50% level)

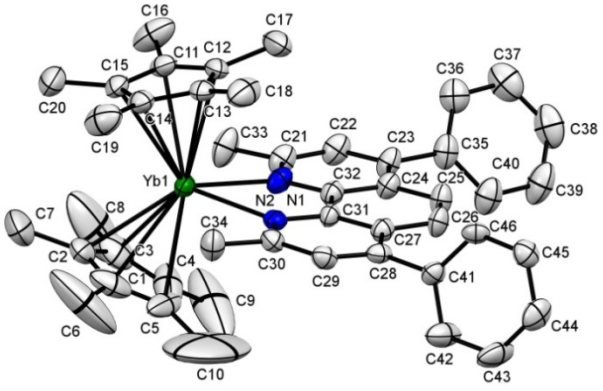

Figure 5. ORTEP for the complex $Cp^*_2Yb(2,9\text{-}Me_2\text{-}4,7\text{-}Ph_2phen)$ (**5**). (Thermal ellipsoids are at 50% level)

Table 4. Bond Lengths (Å) Changes $\Delta^{a,b}$ in **2**, **5** and $Cp^*_2Yb(phen)$.

Bond[c]	$Cp^*_2Yb(4,7\text{-}Me_2phen)$ (**2**)	$Cp^*_2Yb(phen)$[6]	$Cp^*_2Yb(2,9\text{-}Me_2\text{-}4,7\text{-}Ph_2phen)$ (**5**)
A	-0.018	-0.020	-0.018
I	+0.035	+0.014	-0.011
F, L	+0.006	+0.041	-0.006
B, P	+0.019	+0.006	-0.008
H, J	+0.015	-0.026	-0.001

a) Δ is the bond length in the adduct minus that in the free ligand in Å.
b) Free $4,7\text{-}Me_2phen$, ref [13] and for free $2,9\text{-}Me_2\text{-}4,7\text{-}Ph_2phen$, ref [14].
c) The letter refers to the C-C or C-N bond label in Scheme 2.

Although the Yb-C(Cp*) and Yb-N distances in $Cp^*_2(4,7\text{-}Me_2phen)$, **2**, are longer that those in $Cp^*_2Yb(phen)$, the C–C and C–N distances in the phenanthroline ligands are consistent with occupation of the b_1 and a_2 symmetry orbitals.. Using the method outlined in an earlier article,[6] the distances labeled A, I, F and L, B and P, H and J (Scheme 2) change in opposite directions depending on whether the b_1 or a_2 orbitals are populated (See Scheme 1 and Table 4 of ref[6]). The bond length alteration for $Cp^*_2(4,7\text{-}Me_2phen)$, **2**, and $Cp^*_2(phen)$, monomer, indicate that both of these symmetry orbitals are populated but the relative values of Δ are different, implying that the relative energy of these orbitals depend on the position of the methyl groups in the ring. Although these bond length changes are only qualitative, they point towards population of the a_2 orbital in which the coefficient for the carbon pπ-orbitals in the 4,7-positions in the ring are greater than that in b_1; this difference has ramifications for the reactivity at these positions, see below.

Solutions properties. The UV-Vis spectra at 20 °C in toluene for the $4,7\text{-}Me_2phen$ and related adducts are shown in Figure 6. The absorption around 550 nm is due to the π–π* transition in the radical-anion.[15]

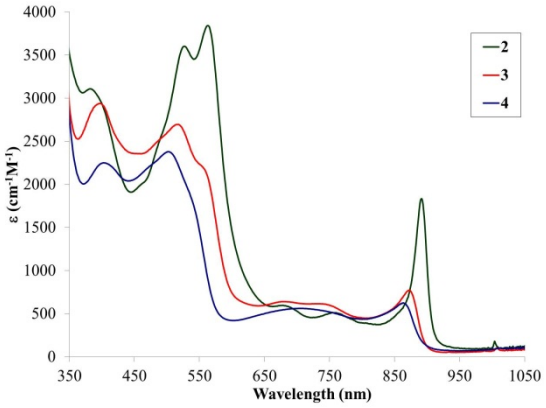

Figure 6: UV-Vis spectra of $Cp^*_2Yb(4,7\text{-}Me_2phen)$, **2**, (green), $Cp^*_2Yb(3,4,7,8\text{-}Me_4phen)$ (red), **3**, $Cp^*_2Yb(3,4,5,6,7,8\text{-}Me_6phen)$, **4**, (blue).

These adducts also have an intense absorption around 900 nm, which was assigned to a f-f transition in $Cp^*_2Yb(phen)$.[15] Although this transition is forbidden, its intensity is attributed to the formation of a ligand-to-metal charge transfer state, ^{1}LMCT, in which intensity is stolen.[15]

The solution ^{1}H NMR spectra in C_6D_6 at 20 °C for the dimethylphenanthroline adducts are listed and assigned in Table 5. The assignments are made by the changes that results when a pair of hydrogens is replaced by a pair of methyl groups at a given position in the phenanthroline ring. Three patterns emerge from the changes in the chemical shift values. (i) The values of $\delta_{2,9}$ are strongly shifted downfield, consistent with the dipolar contribution dominating the chemical shift tensor. This is expected since the dipolar contribution is related to the geometry of the hydrogen atoms and $H_{2,9}$ are proximal to the paramagnetic center. The chemical shifts of $\delta_{2,9}$ also aligns the magnetic z-axis collinear with the N-N vector and perpendicular to C_t-Yb-C_t. (ii) The values of $\delta_{4,7}$ and $\delta_{3,8}$ are less strongly shifted downfield and when the $H_{4,7}$ or $H_{3,8}$ are replaced by methyl groups, the sign of the chemical shift changes showing that the contact contribution to the chemical shift tensor dominates the dipolar contribution.[16] (iii) The $\delta_{5,6}$ values are the farthest upfield and the sign does not change when $H_{5,6}$ is replaced by methyl groups.

In the neutral adducts, the order of chemical shift is $\delta_{2,9} > \delta_{4,7} > \delta_{3,8} > \delta_{5,6}$ but in the cation, the order of $\delta_{4,7}$ and $\delta_{3,8}$ exchange places consistent with the dipolar contribution dominating the chemical shift tensor in the cation. The value of δ_{Cp^*} in the neutral and cation adducts, is around 4 ppm in all cases.

It is informative to compare the chemical shifts of the neutral bipyridine and the neutral phenanthroline adducts of Cp^*_2Yb using the graphic in Scheme 3.

Scheme 3.

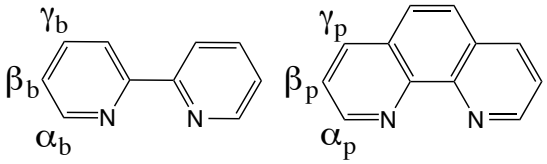

Table 5. ^{1}H NMR chemical shifts (δ) of the phenanthroline adducts at 300K.[(a)]

Compound	2,9	4,7	3,8	5,6	Cp*	ref
$Cp^*_2Yb(phen)$-monomer[b)]	139.9	47.9	14.0	0.47	4.11	ref[6]
$Cp^*_2Yb(4,7\text{-}Me_2phen)$ [b)]	109.1	-21.4(Me)	16.7	3.15	3.63	This work
$Cp^*_2Yb(3,8\text{-}Me_2phen)$ [b)]	95.5	51.1	-10.0 (Me)	3.83	3.36	ref[6]
$Cp^*_2Yb(5,6\text{-}Me_2phen)$ [b)]	137.4	44.1	14.7	0.03 (Me)	3.95	ref[6]
$[Cp^*_2Yb(4,7\text{-}Me_2phen)]I$ [c)]	301	8.4 (Me)	53.4	-3.5	3.73	This work

[Cp*$_2$Yb(phen)]I [c)]	281	9.5	52.4	-2.5	3.82	ref[6]

a) δ value in ppm relative to Me_4Si b) in C_6D_6 or C_7D_8 c) in CD_2Cl_2

The labels α, β, γ are the hydrogen on the alpha, beta and gamma carbon atoms relative to N and b is for bipyridine and p for phenanthroline. The values of the chemical shift at 20 °C in C_6D_6 for Cp*$_2$Yb(bipy)[4,5] and Cp*$_2$Yb(phen)[6] are, to the nearest whole number, α_b, 160; β_b, 6; γ_b, 26, in the bipyridine complexes and α_p, 140; β_p, 14; γ_p, 48 in the phenanthroline complexes. In the bipyridine and phenanthroline adducts $\delta_\alpha >> \delta_\beta < \delta_\gamma$, with δ_α in each adduct approximately equal but δ_β and δ_γ in the phenantholine complexes being about twice the value of δ_β and δ_γ in the bipyridine complexes. Since the chemical shift of the hydrogens on the β and γ sites are largely determined by the contact contribution, this implies that the unpaired spin density at the γ site is greater than that at the β site, and is greater in the phenantholine complexes than in the bipyridine complexes; as mentioned above, this difference plays a role in the reactivity at these positions, see later

Calculations. As in earlier articles on the bipyridine adducts, the CASSCF methodology is used to determine the ground state electronic structure of the phenanthroline adducts of Cp*$_2$Yb.[1-4,6] The phenanthroline adduct of Cp*$_2$Yb is calculated to consist of a pair of nearly degenerate triplets, T1 and T2, which are 2.1 eV below the open-shell singlet exited state.[6] When two methyl groups are attached to the 3,8 and 5,6 positions in the phenanthroline ligand, the ground state of the adducts is still a triplet but the open-shell singlet excited state is now only 0.08 and 0.09 eV above the triplet. In these compounds, the f^{13} configuration is the only active one and the ytterbium atoms are fully trivalent; the computational results are in agreement with the magnetic and XANES experiments for these adducts.[6] In contrast, the calculated ground state of the 4,7-Me$_2$phen adduct is not a triplet but consists of three open-shell singlets, SSI, SS2 and SS3 that are lower in energy relative to the triplet by 0.44 eV, 0.06 eV and 0.02 eV, respectively. The three open-shell singlets have different contribution of f^{13} and f^{14} from Yb and π^*_1 and π^*_2 contributions from the radical anionic ligands and both are therefore multiconfigurational singlets. The SS1, SS2, and SS3 states are given by 0.92 f^{13} + 0.08 f^{14}, 0.34 f^{13} + 0.66 f^{14} and 0.63 f^{13} + 0.37 f^{14}, respectively. The π^*_1 and π^*_2 contribution to SS1 is 0.89 π^*_1 + 0.11 π^*_2 and for SS2 and SS3, the contributions are 0.35 π^*_1 + 0.65 π^*_2 and 0.68 π^*_1 + 0.32 π^*_2, respectively. The most stable state, SS1, is dominated by f^{13} and π^*_1 configurations and in the nearly degenerate SS2 and SS3 states, these configurations are less dominant. For SS1, the n_f value is 0.92, the value of c_1^2 in $\Psi = c_1|Yb(III, f^{13})(phen^{\bullet-}) > + c_2|Yb(II, f^{14})(phen)^0 >$, such that $n_f = 1$ when $c_1=1$ and $c_2 = 0$ and $n_f = 0$ when $c_1 = 0$ and $c_2 = 1$. The calculated value of n_f for SS1 of 0.92 is in reasonable agreement with the experimental value of 0.81 at low temperature, assuming that only SS1 is populated. As the temperature is increased the n_f value of the excited state decreases to 0.58, in reasonable agreement with the calculated values of SS2 and SS3, where the average values in these two states is 0.48.

Reactivity. As mentioned in the Synthesis Section above, the yield of Cp*$_2$Yb(4,7-Me$_2$phen), **2**, is higher and purification is easier when the temperature is kept at 0 °C. In the synthesis of the other two adducts of Me$_4$phen and Me$_6$phen the temperature must be maintained at −70 °C during the synthesis stage. It was not clear why the temperature is important until the thermal stability of isolated Cp*$_2$Yb(4,7-Me$_2$phen), **2**, was monitored by ^{1}H NMR spectroscopy as a function of time. At 60 °C, the resonances of Cp*$_2$Yb(4,7-Me$_2$phen), **2,** in C_7D_8 disappear while a new set appears, a transformation that is complete over 15 days. The ^{1}H NMR spectrum is complex but two different set of resonances can be identified, labeled A_1 and A_2, since the ligand resonances are asymmetric, and the Cp* resonances appear as a broad feature at ~ 3.7 ppm. The spectrum is available in SI. Although the resonances cannot be conclusively assigned, they may be tentatively assigned as due to a hydrogen atom transfer reaction analogous to that illustrated in Scheme 1, as shown in the Experimental Section, Scheme 7. This attribution is supported by the following experiments.

1. The thermal reaction conducted on a synthetic scale yields brown crystals isolated by crystallization from toluene solution (referred to as **7**). The ^{1}H NMR spectrum contains the resonances referred to as A_1 and A_2, above. A brown crystal was selected and an X-ray data set was collected (see Figure 7). Analysis of the X-ray data indicated the presence of two different molecules that co-crystallize in a 72:28 ratio. The major one consists of a dimethylphenanthroline group that has lost a H atom from a methyl group leading to a terminal methylene represented in pink in Figure 7 (C28 and C34) (Scheme 4). The minor molecule consists of a dimethylphenanthroline to which a H atom is added to the phenanthroline ring at carbon C28. This leads to a C(Me)(H) group in two possible positions at C28 (up and down). This position disorder is represented in orange in Figure 7 (Scheme 4) (C28A-C34A and C28B-C34B). Details of the crystallographic solution are given in the Experimental Section and in SI.

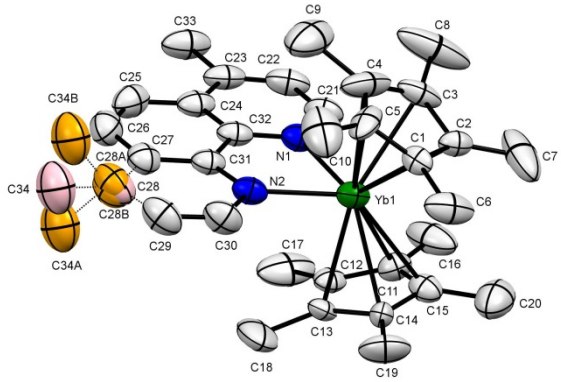

Figure 7. ORTEP for the brown crystal obtained from toluene in the thermal reaction of Cp*$_2$Yb(4,7-Me$_2$phen), **2** (thermal ellipsoids are at 50% level) and referred to as "compound" **7**. The carbon atoms represented in orange are due to a positional disorder of a methyl group connected to the phenanthroline ring and the carbon atom represented in pink is due to the methylene group.

Scheme 4.

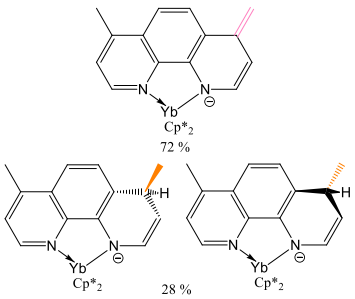

In both cases, a pyridyl ring has lost its aromaticity that results in a shorter Yb-N(2) distance of 2.286(3) Å compared to Yb-N(1) distance of 2.363(3) Å, a consequence of the localization of negative charge on the nitrogen N(2) (Figure 7).Washing the brown crystals with pentane results in a purple solution and a green residue. Cooling the pentane solution (-20 °C) afforded very small crystals (too small for conventional X-ray crystallographic use), but whose ^{1}H NMR spectrum in C_7D_8 is identical to those labeled as A_1, with the exception that the Cp* resonances are resolved as two singlets at δ = 3.94 ppm and 3.58 ppm due to 15 protons each.

2. Hydrolysis (H_2O) of the products of thermal transformation, on a NMR tube scale, results in an asymmetric set of ^{1}H resonances due to H_2A_1, that is , 4,7-Me_2phen+2H's, which evolve into resonances due to 4,7-Me_2phen over one day. No resonances attributable to A_2 are identified. Examination of the solution by GCMS showed Cp*H and 4,7-Me_2phen. When the thermal transformation is monitored by ^{1}H NMR spectroscopy in C_7D_8 in presence of excess dihydroanthracene or 1,4-cyclohexadiene, neither anthracene nor benzene are detected in the spectrum and the $t_{1/2}$ of the reaction is not altered by these two free radical traps. Monitoring the transformation in an atmosphere of D_2 also did not alter the rate but HD is indeed observed. These experiments do not identify A_1 and A_2 with confidence but allow us to ascribe them as resulting from a disproportionation reaction analogous to that shown in Scheme 1.

Discussion. The key point that emerges when the bipyridine and phenanthroline adducts of Cp^*_2Yb are compared is that the bipyridine adducts are all open-shell singlets but the phenanthroline adducts are either open-shell multiconfigurational singlets in Cp^*_2Yb(4,7-Me_2phen) **2**, or triplets in the phenanthroline, 3,8-Me_2phen, and 5,6-Me_2phen adducts. Thus, two methyl groups in different positions on the phenantholine ligand change the magnetic properties of the resulting adduct. A qualitative MO model was presented to account for the difference between Cp^*_2Yb(bipy) and Cp^*_2Yb(phen), which are ground state singlets and triplets, respectively.[6] The model is straightforward for bipyridine, since only the b_1-orbital is low enough in energy to accept an electron in the charge transfer ground state resulting in a singlet state. In the phenanthroline radical anion, the LUMO and LUMO + 1 orbitals of b_1 and a_2 symmetry (in C_{2v} symmetry) are low enough in energy to be populated in the charge-transfer ground state of the adducts resulting in a triplet state, as shown in the left-hand side of the diagram in Figure 8. The spin state of Cp^*_2Yb(x,x'-phen) is qualitatively determined by the energy that separates the b_1 and a_2 symmetry orbitals. When the separation is on the same order or smaller than in phenanthroline, a triplet state results when x,x' is 3,8 or 5,6, as shown in the left-hand side of the diagram in Figure 8, since the symmetry of the SOMOs (singly occupied molecular orbitals) is different and the spins of the electrons in these orbitals can have the same sign. When the separation is larger, the spin arrangement approaches that of Cp^*_2Yb(bipy), resulting in a singlet ground state, as shown in the right-hand side of Figure 8, since the symmetry of the SOMOs is the same and the electrons in them cannot have the same sign.

A model to account for the energy separation between the b_1 and a_2 orbitals, based on the CI calculations, is presented as a guide to understand how the methyl groups can control the spin state in the Cp^*_2Yb(x,x'-phen). Figure 9 shows a cartoon energy-level diagram that is modified from Figure 8 in ref [4]. The diagram illustrates how the open-shell singlet, OSS, and the closed-shell singlet, CSS, energy levels mix under configuration interaction. The diagram is idealized since it only shows a singly occupied f-electron interacting with a single electron in a π* orbital and how these two orbitals change when CI is turned on as the triplet state energy is held constant.

The energy separation, Δ_{SS}, on the left-hand side of Figure 9 represents the large separation in OSS and CSS in Cp^*_2Yb(phen). Replacing two hydrogens by methyl groups on the phenanthroline ligand reduces ΔSS since the methyl group is a σ-donor relative to hydrogen. This raises the energy of the HOMO of the ligand, moving it closer to the energy of the empty d-parentage orbital of Cp^*_2Yb(II, f^{14}) as the bond develops, and stabilizing the configuration. In addition, the methyl substituents raise the LUMO of the ligand, driving up the π* orbital energy, as shown by the increased value of $E_{1/2}$, relative to $Fc^{0/+}$. The values in thf for phen and 3,4,7,8-Me_4phen are -2.55 and -2.68 V, respectively.[9]

Scheme 5.[6]

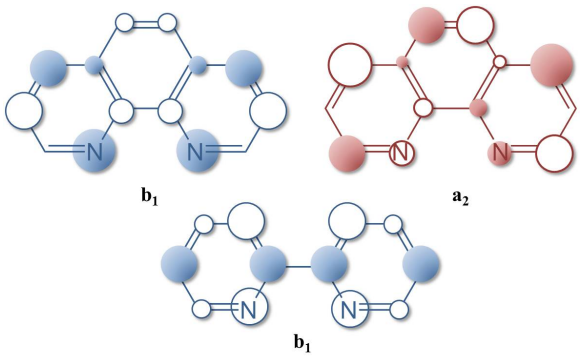

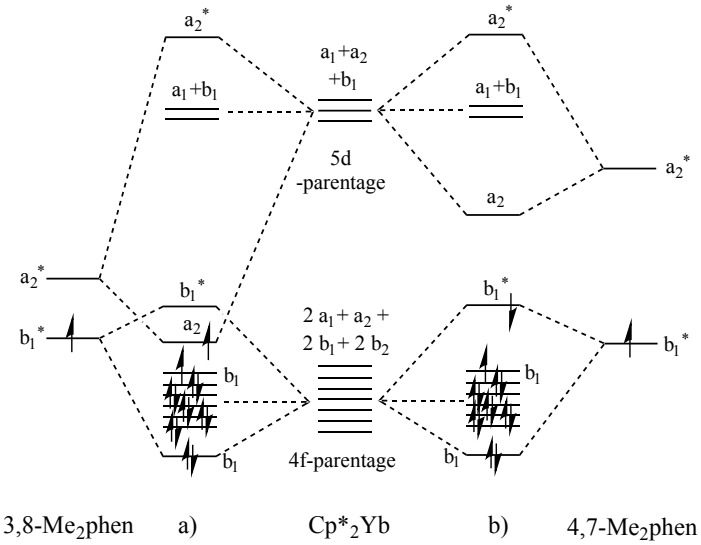

Figure 8. Qualitative MO diagram comparing bonding in $Cp^*_2Yb(3,8\text{-}Me_2phen)$ (a) and $Cp^*_2Yb(4,7\text{-}Me_2phen)$. The 4f-parentage orbitals in the center of the MO-diagram are associated with the Cp^*_2Yb-fragment in C_{2v} symmetry; the two sigma bonding and antibonding orbitals used in bonding of Cp^*_2Yb to the diimine ligands are are not shown, but the three empty d-parentage orbitals are shown. The orbitals on the extreme left-and and right-hand side are the LUMO and LUMO + 1 of the diimine ligands. The orbitals shown in (a) and (b) are the two possible electron configurations in the charge-transfer state of the adducts.

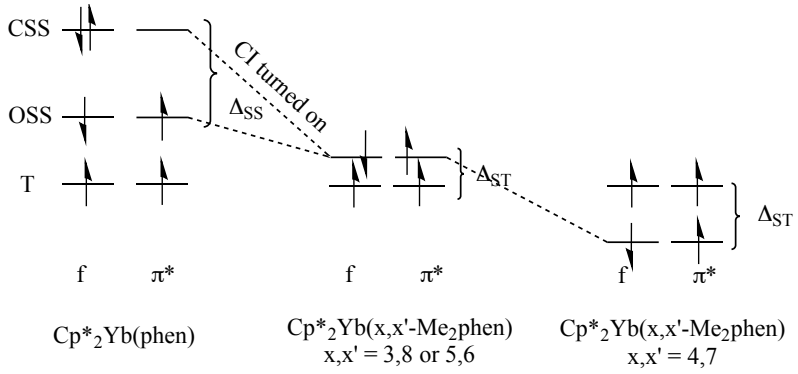

Figure 9. Cartoon energy-level diagram demonstrating the effect of singlet - triplet configurations; close-shell singlet, CSS, open-shell singlet, OSS, and triplet, T, on a singly occupied f orbital coupled with one unpaired electron in a ligand π* orbital. The orbital energies are only qualitative, but they reflect the CASSCF energies.

The reduction potential for the other dimethylphenanthrolines are not available in the literature. The σ-donor substituent destabilizes OSS with the net effect that Δ_{SS} gets smaller, when CI is turned on, driving the energy separation between the singlet and triplet state energies, Δ_{ST}, closer to each other, as in the middle illustration in Figure 9. The qualitative picture agrees with the calculated separation between the singlet-triplet state in the phen, 3,8-Me_2phen, and 5,6-Me_2phen, with the triplet state lower in energy. As Δ_{SS} continues to contract, the multiconfigurational state, composed of the OSS and CSS configurations, falls below the triplet state, as found in the calculation for $Cp^*_2Yb(4,7\text{-}Me_2phen)$, **2**. A qualitative picture for these energy changes is provided by inspection of the relative coefficients on the carbon-p_x orbitals on the b_1- and a_2-symmetry orbitals. The coefficient on the carbon p_x orbitals in the 5,6-positions of b_1-orbital are small, the a_2-orbital has a node in the 3,8-positions, and the coefficient in the 4,7-positions in both orbitals is large, Scheme 5. The net effect is that methyl groups occupying the 3,8- and 5,6-positions destabilize the OSS state. The destabilization is substantially larger in both orbitals when methyl groups occupy the 4,7-positions, lowering the ΔSS and driving the multiconfigurational singlet state below the triplet when CI is turned on. As more methyl groups replace hydrogens in the phenanthroline ligand, the stabilization continues, consistent with the experimental results in Table 2.

The change in the electronic structure of the adducts plays a key role in determining the site of reactivity in the phenanthroline adducts. Thus, $Cp^*_2Yb(phen)$ and $Cp^*_2Yb(3,8\text{-}Me_2phen)$ are dimers in the solid state due to formation of a σ-C–C bond between the carbon atoms in the 4-position of the phenanthroline ligand.[6] The 3,8-Me_2phen adducts exists in a dimer ⇌ 2 monomer equilibrium in solution but the insolubility of the phen adduct prevents the acquisition of an equilibrium constant. In the solid state structures of these dimers, the C–C bond length is longer and presumably weaker in the 3,8-Me_2phen dimer than in the unsubstituted phen dimer, likely due to steric repulsion between the two monomeric units in the dimer. Steric repulsion is presumably a factor contributing to the monomeric solid state structure of $Cp^*_2Yb(5,6\text{-}Me_2phen)$ as well as the distribution of the unpaired spin density at the 4-carbon –pπ orbital.[6]

When two methyl groups are located on the 4,7-positions, the repulsion between the methyl groups in a hypothetical dimer is larger than the stabilization resulting from σ-C–C bond formation. The increase in spin density on the carbon p_x-orbitals at the 4,7-positions is relieved by delocalization of the spin density in the p_x-orbital into the σ*-C–H bonds of a methyl group. This delocalization results in weakening the C–H bond of the methyl group and strengthening the C=C bond as the negative charge in the pyridyl ring rearranges forming A_1 and A_2 in the Cp^*_2Yb adducts, as well in the Cp_2Ti adducts.[11]

The qualitative picture that is outlined above also fits the experimental observation that $Cp^*_2Yb(4,4'\text{-bipy})$ is a thermally stable monomer but $Cp^*_2Yb(4,7\text{-}Me_2phen)$ is not, even though both have open-shell singlet multiconfigurational ground states and a similar value of n_f. Inspection of the b_1-symmetry orbitals in both ligands provides a possible answer: the coefficients of the p_x-carbon orbitals on the p_x C-4 position in each radical anion is smaller in bipy·- than in phen·-. This difference results in localization of less spin density on a given carbon atom in bipy·- and a smaller driving force for C–C bond formation or C–H bond breaking. This conjecture, *viz.*, the spin density distribution in the radical anions means that determining the experimental spin density map in these radical anions is the next step in unraveling the physics and chemistry of these molecules.

Three possible mechanisms may be considered for the reaction illustrated in Scheme 1: (i) an intramolecular free radical process, (ii) an intermolecular radical-pair process, and (iii) an intermolecular proton transfer process. A free radical mechanism is ruled out by the results of the radical trapping experiments, which leaves the intermolecular pathways in which a hydrogen atom (ii) or a proton (iii) is transferred. These two processes are illustrated in Scheme 6. The pathways differ by the nature of the σ-C–C bond between the two radical anions; in (ii) the spins are weakly correlated as in a pair of radicals and in (iii) the spins are more strongly correlated as in a bond. The experimental information does not allow a distinction to be made, but the formation of HD when D_2 is present seems to favor the proton transfer mechanism.

Scheme 6.

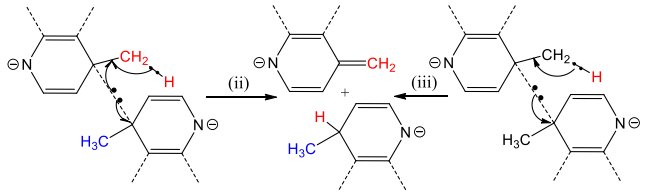

Conclusion. The ground state electronic structure of the paramagnetic charge-transfer diimine adducts of Cp^*_2Yb range from open-shell singlets to triplets depending on the identity of the diimine and the number and position of methyl substituents in the diimine. The different electronic structures are perhaps, surprising, since the neutral ligands have similar donor and acceptor properties[17] and the magnetic properties are determined by the symmetry and energy of the SOMO orbital(s) in the radical anion. All of the 2,2'-bipyridine adducts studied have open-shell singlet ground states whose wave function is described by $\Psi = c_1|Yb(III, f^{13})(bipy^{\bullet-})> + c_2|Yb(II, f^{14})(bipy)^0>$.[4] All of the methyl and dimethyl bipy adducts are open-shell singlets in which the coefficients c_1 and c_2 depend on their position in the ring.[3] In contrast, the various phenanthroline adducts range from a triplet, $c_2 = 0$, when 1,10-phenanthroline is the diimine,[6] to open-shell singlets in the $4,7\text{-}Me_2phen$ adduct. The origin of this difference is traced to the energy separation between the open-shell singlet (Yb↑ L↓) and the close-shell singlet (Yb↑↓ L^0) and therefore their extent of configuration-interaction mixing, which depends on the number and position of the methyl groups in the ring. The electronic structure of these phenanthroline adducts alters their reactivity patterns. For example, the $3,8\text{-}Me_2phen$ adduct exists in a dimer-monomer equilibrium in solution in which the σ-C–C bond that connects the monomeric halves in the dimer is weak; the BDE is *ca.* 8 $kcal^{-1}mol^{-1}$.[6] The $4,7\text{-}Me_2phen$ adduct undergoes an irreversible disproportionation in solution in which one C–H is broken while another one is formed, Scheme 6. A tentative suggestion is offered for the different reactivity patterns that involves the extent of unpaired spin density in the carbon p_x-orbital on the 4 and 7-positions. This postulate, if true, provides a way to control the reactivity patterns in these organometallic compounds.

EXPERIMENTAL SECTION.

General considerations. All reactions were performed using standard Schlenk-line techniques or in a drybox (MBraun). All glassware was dried at 150 °C for at least 12 h prior to use. Toluene, pentane, and diethyl ether were dried over sodium and distilled while CH_2Cl_2 was purified by passage through a column of activated alumina. Toluene-d_8 and CH_2Cl_2-d_2 were dried over sodium. All the solvents were degassed prior to use. ^1H NMR spectra were recorded on Bruker AVB-400 MHz, DRX-500 MHz, AVB-600 MHz and Advance 300 MHz spectrometers. ^1H chemical shifts are in δ units relative to TMS, and coupling constants (*J*) are given in Hz. Infrared spectra were recorded as Nujol mulls between KBr plates on a Thermo Scientific Nicolet IS10 spectrometer. Samples for UV-Vis-NIR spectroscopy were obtained in a Schlenk-adapted quartz cuvette and obtained on a Varian Cary 50 scanning spectrometer. Melting points were determined in sealed capillaries prepared under nitrogen and are uncorrected. Elemental analyses were determined at the Microanalytical Laboratory of the College of Chemistry, University of California, Berkeley. X-ray structural determinations were performed at CHEXRAY, University of California, Berkeley. Magnetic susceptibility measurements were made for all samples at 1, 5 and 40 kOe in a 7 T Quantum Design Magnetic Properties Measurement System that utilizes a superconducting quantum interference device (SQUID). Sample containment and other experimental details have been described previously.[18] Sample integrity was verified by observing the absorption spectra of an oxygen "canary" that is always loaded into one slot of each multislot sample holder, typically a divalent ytterbocene such as $Cp^*_2Yb(OEt_2)$. Diamagnetic corrections were made using Pascal's constants. The samples were prepared for X-ray absorption experiments as described previously and the same methods were used to protect the air-sensitive compounds from oxygen and water.[4] X-ray absorption measurements were made at the Stanford Synchrotron Radiation Lightsource on beamline 11-2. The samples were prepared and loaded into a liquid helium-flow cryostat at the beamline as described previously.[4] Data were collected at temperatures ranging from 30 to 300 K, using a Si(220) double-crystal monochromator. Fit methods were the same as described previously.[4] Low temperature (ca. 2 K) EPR spectra were obtained with a Varian E-12 spectrometer equipped with an EIP-547 microwave frequency counter and a Varian E-500 gaussmeter, which was calibrated using 2,2-diphenyl- 1-picrylhydrazyl (DPPH, g= 2.0036).

Calculations. The ytterbium center was treated with a small-core relativistic pseudopotential (RECP) ([Ar] + 3d)[19] in combination with its adapted basis set (segmented basis set that

includes up to g functions). The carbon, nitrogen and hydrogen atoms were treated with an all-electron double-ζ, 6-31G(d,p),[20] All the calculations were carried out with the Gaussian 03 suite of programs[21] and ORCA suite of program[22] either at the Density Functional Theory (DFT) level using the B3PW91[23] hybrid functional or at the CASSCF level; only one active space and inactive orbitals were used in the calculation. The geometry optimizations were performed without any symmetry constraints at either the DFT or the CASSCF level. The electrons were distributed over four 4f orbitals and the two π* orbitals of phenanthroline.

Syntheses. The ligands, 3,4,7,8-tetramethylphenanthroline (3,4,7,8-Me_4phen), 2,9-dimethylphenanthroline (2,9-Me_2phen), 4,7-dimethylphenanthroline (4,7-Me_2phen), and 2,9-dimethyl-4,7-diphenylphenanthroline (2,9-Me_2-4,7-Ph_2phen) were bought from Aldrich. 3,4,5,6,7,8-Hexamethylphenanthroline (3,4,5,6,7,8-Me_6phen) was a gift from Prof. S.J. Buchwald at MIT. All ligands were purified by sublimation between 80 and 200°C prior to use.

Cp^*_2Yb(2,9-Me_2phen) (1). The complex $Cp^*_2Yb(OEt_2)$ (0.222 g, 0.430 mmol) was combined with 2,9-dimethyl-1,10-phenanthroline (2,9-Me_2-phen, 0.089g, 0.429 mmol) and toluene (30mL) was added at room temperature. The pink/purple solution was stirred for 2 h at room temperature. A dark precipitate formed. The suspension was cooled at -20°C and the dark powder was collected by filtration (198 mg, 71%). The dark powder was purified by crystallization in hot toluene (10 mL) (145 mg, 52 %). X-ray quality crystals were obtained by this method. ^{1}H NMR: (toluene-d_8, 300K, δ (ppm) 12.94 (2H, d, J= 6.8, phen), 8.57 (2H, d, J= 6.8, phen), 7.29 (6H, Me-phen), 6.88 (2H, s, phen), 1.84 (30H, C_5Me_5). mp: 313-317°C. Anal. Calcd for $C_{34}H_{42}N_2Yb$: C, 62.66; H, 6.50; N, 4.30. Found: C, 62.74; H, 6.31; N, 4.12. IR: 1622 (w), 1592 (w), 1505 (m), 1435 (s), 1374 (m), 1354 (w), 1316 (vw), 1300 (vw), 1206 (vw), 1148 (m), 1027 (m), 848 (s), 814 (vw), 784 (vw), 730 (s), 694 (w), 637 (w).

Cp^*_2Yb(4,7-Me_2phen) (2). The complex $Cp^*_2Yb(OEt_2)$ (0.373 g, 0.721 mmol) was combined with 4,7-dimethyl-1,10-phenanthroline (4,7-Me_2phen, 0.150 g, 0.721 mmol) and toluene (50 mL) was added at O °C. The deep purple solution was stirred for 8 h at 0 °C, concentrated to 15 mL, warmed to room temperature to dissolve the dark residue and slowly cooled at -20 °C. Dark purple-red crystals suitable for X-ray diffraction formed overnight (295 mg, 63%). ^{1}H NMR in C_6D_6, elemental analysis and X-Ray diffraction indicates the presence of half a molecule of toluene. ^{1}H NMR: (toluene-d_8, 300 K) δ (ppm) 109.13 (2H, 2,9-phenH), 16.69 (2H, 3,8-phenH), 3.63 (30H, C_5Me_5), 3.15 (2H, 5,6-phenH), -21.35 (6H, 4,7Me-phen). mp: 265-268°C. Anal. Calcd for $C_{37,5}H_{46}N_2Yb$: C, 64.54; H, 6.64; N, 4.01. Found: C, 64.13; H, 6.11; N, 3,98. IR (cm^{-1}): 1622 (m), 1577 (w), 1520 (m), 1436 (m), 1374 (s), 1352 (s), 1256 (m), 1221 (m), 1183 (m), 1145 (s), 1077 (m), 981 (s), 849 (s), 790 (m), 728 (m), 694 (w).

Cp^*_2Yb(3,4,7,8-Me_4phen) (3). The complex $Cp^*_2Yb(OEt_2)$ (0.114 g, 0.221 mmol) was dissolved in Et_20 (5 mL) at -77°C and added dropwise over 30 min to a cold ether suspension (10 mL, -77°C) of 3,4,7,8-tetramethyl-1,10-phenanthroline (3,4,7,8-Me_4phen, 0.056 g, 0.221 mmol). The color of the suspension turned to brown. After the addition was complete, the dark brown reaction mixture was stirred at -77°C for two hours. No color change was observed during this time. The dark brown suspension was allowed to warm to -40°C while the solvent was removed under reduced pressure to ca. 3 mL. The suspension was stored overnight (16h) at -40 °C and a brown powder formed that was collected by filtration at -77°C. The dark brown powder (141 mg, 85%) was washed with cold pentane (3x5 mL) at -77°C and dried under reduced pressure. ^{1}H NMR: (Toluene-d_8, 300K) δ (ppm) 50.40 (2H, phen), 6.54 (2H, phen), 2.64 (30H, C_5Me_5), -6.54 (6H, Me-phen), -16.46 (6H, Me-phen). mp. 264-266°C. Anal. Calcd for $C_{36}H_{46}N_2Yb$: C, 63.63; H, 6.77; N, 4.13. Found: C, 63.90; H, 6.81; N, 4.39. IR (cm^{-1}): 1611 (w), 1567 (w), 1418 (s), 1465 (m), 1438 (w), 1276 (m), 1232 (m), 1176 (m), 1088 (m), 1009 (m), 970 (m), 950 (vw), 907 (wv), 810 (s), 733 (w), 721 (s), 669 (m), 633 (m).

Cp^*_2Yb(3,4,5,6,7,8-Me_6phen) (4). The complex $Cp^*_2Yb(OEt_2)$ (0.086 g, 0.166 mmol) was dissolved in Et_20 (2 mL) at -77°C and added dropwise over 30 min to a cold ether suspension (10mL, -77°C) of 3,4,5,6,7,8-hexamethyl-1,10-phenanthroline (3,4,5,6,7,8-Me_4phen, 0.0323 g, 0.166 mmol). The color of the suspension turned to deep green and then to brown. After the addition was complete, the dark brown reaction mixture was stirred at -77°C for two hours. No color change was observed during this time. The suspension was filtered at -77°C and the green-brown residue was washed with cold ether (-77°C, 3x3mL) and dried under reduce pressure (74mg, 70%). ^{1}H NMR: (Toluene-d_8, 300K) δ (ppm) 42.54 (2H, phen), 2.46 (30H, C_5Me_5), 1.50 (6H, Me-phen), -5.71 (6H, Me-phen), -12.44 (6H, Me-phen). mp. 270-272°C. Anal. Calcd for $C_{38}H_{50}N_2Yb$: C, 64.48; H, 7.12; N, 3.96. Found: C, 64.80; H, 6.85; N, 4.10.

Cp^*_2Yb(2,9-Me_2-4,7-Ph_2phen)·xPhMe (x = 0.25 to 0.5) (5). The complex $Cp^*_2Yb(OEt_2)$ (0.240 g, 0.464 mmol) was combined with 2,9-dimethyl-4,7-diphenyl-1,10-phenanthroline (2,9-Me_2-4,7-Ph_2phen, 0.167g, 0.464 mmol) and toluene (20mL) was added at room temperature. The dark purple solution was stirred for 16h at room temperature, concentrated to the ca. 7 mL and cooled at -20°C. Larges dark purple X-Ray suitable crystals formed overnight. Two crops were obtained, which were combined and re-crystallized in toluene at -20°C (256 mg, 69%). ^{1}H NMR spectra and combustion analysis on the bulk indicated the presence of 0.25 molecule of toluene per complex; however, in the X-ray experiment 0.5 molecule of toluene was found in the unit cell. ^{1}H NMR: (toluene-d_8, 300K): 16.94 (6H, Me), 10.70 (2H, phen-$H_{3,8}$), 8.11 (t, J=7.2 Hz, 2H, H_{para}), 7.88 (d, J=7.6 Hz, 4H, H_{ortho}), 6.83 (t, J=7.2 Hz, 4H, H_{meta}), 6,83 (2H, phen-$H_{5,6}$), 1.72 (30H, Cp*). mp: 288-290°C. Anal. Calcd for $C_{47.75}H_{52}N_2Yb$: C, 69.35; H, 6.34; N, 3.39. Found: C, 69.12; H, 6.10; N, 3.37. IR (cm^{-1}): 1622 (m), 1569 (w), 1547 (m), 1487 (m), 1439 (m), 1411 (w), 1379 (w), 1355 (w), 1261 (vw), 1077 (w), 1027 (m), 100 (m), 880 (s), 842 (vw), 831 (s), 772 (s), 729 (s), 703 (s).

$[Cp^*_2Yb(4,7\text{-}Me_2phen)]^+I^-$ (6). The complex $Cp^*_2Yb(OEt_2)$ (0.174g, 0.337 mmol) was combined with 4,7-dimethylphenanthroline (0.070g, 0.337 mmol) and AgI (0.079g, 0.337 mmol). Toluene (30mL) was added at room temperature and the purple solution was stirred for 16h at room temperature (overnight). The volatile material was removed under reduced pressure and the brown residue was triturated in pentane and extracted in CH_2Cl_2. The orange solution was concentrated to ca. 5 mL and cooled to -20°C. Large gold yellow crystals formed (134 mg, 52%). mp: 214-218°C. ^{1}H NMR: (CD_2Cl_2, 300 K, δ (ppm)) 295.6 (2H, phen) 52.45 (2H, phen), 8.41 (6H, phen), 3.69 (30H, Me_5C_5), -2.89 (2H, phen). Anal. Calcd for $C_{34}H_{42}N_2YbI{\bullet}CH_2Cl_2$: C, 48.68; H, 5.14; N, 3.24. Found: C, 49.47; H, 5.56; N, 3.06. IR (cm^{-1}): 1631 (w), 1534 (w), 1430 (s), 1417 (m), 1377 (w), 1332 (m), 1301 (w), 1273 (w), 855 (m), 728 (s), 682 (w), 612 (w). EPR (solid 2 K) : g_1 = 7.136, g_2 = 1.829, g_3 = 1.214 ; using these g-values gives μ_{eff} (2 K) = 3.7 μ_B.The value of μ_{eff} (0 K from 12 K to 45 K and extrapolation to 0 K gives μ_{eff} (0 K) = 3.6 μ_B.

Reactivity of the complex Cp^*_2Yb(4,7-Me_2phen).
Scheme 7.

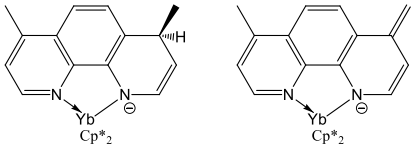

A1 **A2**

^{1}H NMR studies. An NMR tube containing a C_6D_6 solution of the complex $Cp^*_2Yb(4,7\text{-}Me_2phen)$ was heated at 60ºC over a period of 15 days and followed by ^{1}H NMR spectroscopy. The initial set of 5 resonances in a 2:2:2:6:30 ratio decreased in intensity while two new sets of peaks (A_1 and A_2) appeared and increased with time. After 15 days the resonances due to $Cp^*_2Yb(4,7\text{-}Me_2phen)$ had disappeared and only those due to A_1 and A_2 remained in the spectrum. The two sets were associated with the formation of the complexes $Cp^*_2Yb(4,7\text{-}Me_2\text{-}4H\text{-}phen)$ (Set **A1**, Scheme 7) and $Cp^*_2Yb(4\text{-}Me\text{-}7\text{-}(CH_2)\text{-}phen)$ (set **A2**, see Scheme 7) in a 1:1 ratio.

After 15 days: ^{1}H NMR: (C_6D_6) δ (ppm) 192.7 (1H, A_1), 186.8 (1H, A_2), 87.81 (1H, A_1), 83.47 (1H, A_2), 24.11 (3H, A_1), 21.07 (3H, A_2), 14.66 (1H, A_2), 4.88 (1H, A_1), 3.73 (br, $\nu_{1/2}$ = 380Hz, Cp^*, 60H), 0.92 (1H, A_1), -2.54 (1H, A_2), -2.71 (1H, A_1), -10.89 (1H, A_2), -12.86 (1H, A_1), -12.95 (1H, A_2), -22.34 (1H, A_2), -22.87 (3H, A_1). One ^{1}H resonance was missing in each compound; changing the temperature did not help locate them.

The rearrangement was performed in presence of 1,10-dihydroanthracene, 1,4-cyclohexadiene, or D_2. Niether anthracene nor benzene were formed in the two first reactions but the presence of D_2 led to the formation of HD. The half-time of the reaction was concentration dependant but no kinetic rate law could be found to fit the data. The presence of D_2 did not change the half-time at the same concentration.

When only A_1 and A_2 were observed in the ^{1}H NMR spectrum, the mixture was hydrolyzed (H_2O) and the hydrosylate was examined by ^{1}H NMR in C_6D_6. ^{1}H NMR: (C_6D_6) δ (ppm) 9.15 (s, 2H, phen), 8.42 (s, 1H, A_1), 8.03 (s, 2H, phen), 7.55 (s, 2H, phen), 7.06 (d, J = 7.6Hz, 1H, A_1), 7.00 (d, J = 7.8Hz, 1H, A_1), 6.67 (1H, A_1), 5.94 (d, J = 7.2Hz, 1H, A_1), 4.54 (m, 1H, A_1), 3.88 (m, 1H, A_1), 2.84 (s, 6H, phen), 2.22 (s, 3H, A_1), 1.34 (3H, d, J = 6.8Hz, A_1). After 1 day, the A_1 set of resonances disappeared and resonances for free $4,7\text{-}Me_2phen$ ligand, due to the re-aromatization of the negatively charged A_1 and A_2 ligands, appeared. The resonances associated with complex A_2 disappeared too rapidly and were not detected in ^{1}H NMR spectrum. A GCMS identified free $4,7\text{-}Me_2phen$ as the only product formed.

Synthesis of the complex $Cp^*_2Yb(4,7\text{-}Me_2\text{-}4H\text{-}phen)$ (8) (A_1).

The complex $Cp^*_2Yb(OEt_2)$ (0.670 g, 1.30 mmol) is combined with 4,7-dimethyl-1,10-phenanthroline ($4,7\text{-}Me_2phen$, 0.70 g, 1.30 mmol) and toluene (30mL) was added at room temperature. The deep purple solution was stirred for 14 days at 60ºC as the color turned to brown. The solution was concentrated to ca. 10mL, warmed to dissolve the brown residue and the resulting solution was filtered while warm and the filtrate was slowly cooled at -20°C. Dark brown crystals suitable for X-ray formed after 3 days (350 mg, 41%). X-ray diffraction data were collected on one of these crystals, resulting in the ORTEP in Figure 7, The^{1}H NMR spectrum of these brown crystals indicated the presence of A_1 and A_2 in approximately equal amounts. The brown crystals were extracted in pentane and the resulting purple solution was filtered to afford a green brown residue. The pentane solution was concentrated to ca. 10mL and cooled at -20°C. Purple needles appeared after two days that were found to be too small for an X-ray diffraction experiment (78 mg, 20%). ^{1}H NMR: (toluene-d_8, 300K) δ (ppm) 192.7 (1H), 87.81 (1H), 24.11 (3H), 14.66 (1H), 3.94 (Cp^*, 15H), 3.58 (Cp^*, 15H), 0.92 (1H), -2.71 (1H), -12.86 (1H), -22.87 (3H); one 1-H resonance is missing. mp: 257-260°C. EIMS: $\{Cp^*_2Yb(4,7\text{-}Me_2\text{-}4H\text{-}phen)\text{-}H\}$, m/z = 651. Anal. Calcd. for $C_{34}H_{13}N_2Yb$: C, 62.56; H, 6.64; N, 4.29. Found: C, 62.37; H, 6.44; N, 4.02. IR (cm^{-1}): 2963 (m), 2905 (m), 2851 (m), 2723 (w), 1583 (s), 1516 (s), 1485 (m), 1467 (m), 1394 (m), 1374 (m), 1259 (s), 1186 (m), 1152 (m), 1076 (s), 1012 (s), 967 (m), 865 (w), 792 (s), 729 (w), 694 (w).

Reactivity of the complex $Cp^*_2Yb(3,4,7,8\text{-}Me_4phen)$.

Heating a solution of $Cp^*_2Yb(3,4,7,8\text{-}Me_4phen)$ was more complicated than the reaction of $Cp^*_2Yb(4,7\text{-}Me_2phen)$, since several species appear to form, none of which could be identified with confidence. In contrast, heating a solution of $Cp^*_2Yb(3,4,5,6,7,8\text{-}Me_6phen)$ formed only two sets of resonances much like $Cp^*_2Yb(4,7\text{-}Me_2phen)$. However, a conclusive assignment of the two sets was not possible. After 15days: ^{1}H NMR: (C_6D_6) δ (ppm) 232.3 (1H,), 210.0 (1H), 62.85 (3H), 60.01 (3H), 27.20 (3H), 25.32 (3H), 23.45 (3H), 23.31 (3H), 7.66 (3H), 3.92 (3H), 3.48 (br, $\nu_{1/2}$ = 380Hz, Cp^*, 60H), -3.83 (1H), -13.48 (d, J=13Hz, 1H), -14.96 (3H), -17.04 (3H), -23.83 (d, J=12.6Hz, 1H), -27.30 (3H). One 1-H resonance was not found for one of each species.

In all three thermal reactions, the half-time of the reactions was similar when similar concentration were used, $t_{1/2}$ was about 5 days at a 5 mM concentration at 60ºC.

X-Ray Crystallography.

Single crystals of the compounds $Cp^*_2Yb(4,7\text{-}Me_2phen)$, **2**, $Cp^*_2Yb(2,9\text{-}Me_2\text{-}4,7\text{-}Ph_2phen)$, **5** and **7** were coated in Paratone-N oil and mounted on a Kaptan loop. The loop was transferred to either a Bruker SMART 1000 diffractometer,[24] for **5** and a SMART APEX diffractometer for **2** and **7**. Both are equipped with a CCD area detector.[25] Preliminary orientation matrices and cell constants were determined by collection of 10s frames, followed by spot integration and least-squares refinement. Data were intergrated by the program SAINT[26] to a maximum 2θ value of 50.8° for **2**, 51.0° for **5** and 50.8° for **7**. The data were corrected for Lorentz and polarization effects. Data were analyzed for agreement and possible absorption using XPREP. A semi-empirical multi-scan absorption correction was applied using SADABS.[27] This models the absorption surface using a spherical harmonic series based on differences between equivalent reflections. The structures were solved by direct methods using SHELX 2013[28] and the WinGX program.[29] Non-hydrogen atoms were refined anisotropically and hydrogen atoms were placed in calculated positions and not refined.

For **2** and **5**, disordered toluene molecules were found in the lattice and were solved. For **7**, a number of restraints were used in order to refine this structure: (i) a highly disordered solvent molecule was SQUEEZED (ii) two different chemical entities co-crystallized on the same site, in a 72/28 ratio with formulae: $C_{34}H_{41}N_2Yb$ (**A2**) and $C_{34}H_{43}N_2Yb$ (**A1**), respectively. The second one displayed a disorder of the C34 methyl group. In order to anisotropically refine these entities, EADP's were used and DFIX instructions were applied to force the $CH\text{-}CH_3$ groups at C28 in a slightly out of plane conformation. (iii) The Cp* rings also were disordered and were refined as idealized entities using AFIX 9 and SIMU instructions. The resolution of the data did not allow releasing these restraints.

Supporting Information. Information concerning magnetic susceptibility, Vis-NIR spectroscopy, ^{1}H Variable Temperature NMR, X-ray crystallography; crystal data and CIF, CCDC# 1019971, 1019972 and 1019973 (**2**, **5** and **7**).

ACKNOWLEDGMENT

G.N. would like to thank CNRS and Ecole polytechnique for funding. Work at University of California, Berkeley and at Lawrence Berkeley National Laboratory was supported by the Director, Office of Energy Research, Office of Basic Energy Sciences, Chemical Sciences, Geosciences and Biosciences Division, Heavy Element Chemistry Program of the U.S. Department of Energy under Contract No. DE-AC02-05CH11231. X-ray absorption data were collected at the Stanford Synchrotron Radiation Lightsource, a Directorate of SLAC National Accelerator Laboratory and an Office of Science User Facility operated for the U.S. Department of Energy Office of Science by Stanford University. We thank Antonio DiPasquale and Fred Hollander at CHEXRAY Berkeley for their help with crystal structures and Wayne W. Lukens for the EPR spectrum and discussions. L.M. is member of the Institut Universitaire de France. Cines and CALMIP are acknowledged for a generous grant of computing time. L.M. would also like to thank the Humboldt Foundation for a fellowship

REFERENCES

1) Nocton, G.; Booth, C. H.; Maron, L.; Andersen, R. A. *Organometallics* **2013**, *32*, 1150.
(2) Nocton, G.; Booth, C. H.; Maron, L.; Andersen, R. A. *Organometallics* **2013**, *32*, 5305.
(3) Booth, C. H.; Kazhdan, D.; Werkema, E. L.; Walter, M. D.; Lukens, W. W.; Bauer, E. D.; Hu, Y.-J.; Maron, L.; Eisenstein, O.; Head-Gordon, M.; Andersen, R. A. *J. Am. Chem. Soc.* **2010**, *132*, 17537.
(4) Booth, C. H.; Walter, M. D.; Kazhdan, D.; Hu, Y.-J.; Lukens, W. W.; Bauer, E. D.; Maron, L.; Eisenstein, O.; Andersen, R. A. *J. Am. Chem. Soc.* **2009**, *131*, 6480.
(5) Schultz, M.; Boncella, J. M.; Berg, D. J.; Tilley, T. D.; Andersen, R. A. *Organometallics* **2002**, *21*, 460.
(6) Nocton, G.; Lukens, W. L.; Booth, C. H.; Rozenel, S. S.; Melding, S. A.; Maron, L.; Andersen, R. A. *J. Am. Chem. Soc.* **2014**, *136*, 8626.
(7) Kaim, W. *J. Am. Chem. Soc.* **1982**, *104*, 3833.
(8) Koizumi, T.; Yokoyama, Y.; Morihashi, K.; Nakayama, M.; Kikuchi, O. *Bull. Chem. Soc. Jpn.* **1992**, *65*, 2839.
(9) Klein, A.; Kaim, W.; Waldhor, E.; Hausen, H. D. *J. Chem. Soc., Perkin Trans.* **1995**, 2121.
(10) McPherson, A. M.; Fieselmann, B. F.; Lichtenberger, D. L.; McPherson, G. L.; Stucky, G. D. *J Am. Chem. Soc.* **1979**, *101*, 3425.
(11) Corbin, D. R.; Willis, W. S.; Duesler, E. N.; Stucky, G. D. *J. Am. Chem. Soc.* **1980**, *102*, 5969.
(12) Tilley, T. D.; Andersen, R. A.; Spencer, B.; Zalkin, A. *Inorg. Chem.* **1982**, *21*, 2647.
(13) De Silva, C. R.; Maeyer, J. R.; Wang, R.; Nichol, G. S.; Zheng, Z. *Inorg. Chim. Acta* **2007**, *360*, 3543.
(14) Wang, J.; Ye, J.-W.; Wang, Y. *Acta Cryst. E* **2007**, *63*, O2007.
(15) Da Re, R. E.; Kuehl, C. J.; Brown, M. G.; Rocha, R. C.; Bauer, E. D.; John, K. D.; Morris, D. E.; Shreve, A. P.; Sarrao, J. L. *Inorg. Chem.* **2003**, *42*, 5551.
(16) La Mar, G. N.; Horrocks, W. D.; Holm, R. H. *NMR of Paramagnetic Molecules: Principles and Applications*; Elsevier Inc., 1973.
(17) McWhinnie, W. R.; Miller, J. D. In *Adv. Inorg. Chem. and Radiochem.* Emeléus, H. J., Sharpe, A. G., Eds.; Academic Press: 1970; Vol. Volume 12, p 135.
(18) Walter, M. D.; Schultz, M.; Andersen, R. A. *New. J. Chem.* **2006**, *30*, 238.
(19) Dolg, M.; Stoll, H.; Preuss, H. *J Chem. Phys.* **1989**, *90*, 1730.
(20) Harihara P.C., Pople, J. A. *Theor. Chim. Acta* **1973**, *28*, 213.
(21) Frisch, J.; Revision E-01 ed.; Gaussian Inc.: Pittsburgh, PA, 2001.
(22) Neese, F.; Version 2.4. ed.; Chemie, M.-P.-I. f. B., Ed. Mülheim and der Ruhr, 2004.
(23) Becke, A. D. *J. Chem. Phys.* **1993**, *98*, 5648.
(24) Bruker Analytical X-Ray System, I. Madison, Wisconsin, USA, 2007.
(25) Bruker Analytical X-Ray System, I. Madison, Wisconsin, USA, 2007.
(26) Bruker Analytical X-Ray System, I. Madison, Wisconsin, USA, 2007.
(27) Blessing, R. *Acta Cryst. A* **1995**, *51*, 33.
(28) Sheldrick, G. M. *Acta Cryst. A* **2008**, *64*, 112.
(29) Farrugia, L. *J. App. Cryst.* **1999**, *32*, 837.